ORIGINAL ARTICLE

JBMR®

Adding Marrow Adiposity and Cortical Porosity to Femoral Neck Areal Bone Mineral Density Improves the Discrimination of Women With Nonvertebral Fractures From Controls

Roger Zebaze,[1,2]* Marit Osima,[3,4]* Minh Bui,[5] Marko Lukic,[3] Xiaofang Wang,[2] Ali Ghasem-Zadeh,[2] Erik F Eriksen,[6,7] Angela Vais,[8] Catherine Shore-Lorenti,[1] Peter R Ebeling,[1] Ego Seeman,[2,9] and Åshild Bjørnerem[10,11]

[1]Department of Medicine, School of Clinical Sciences, Monash Health, Monash University, Melbourne, Australia
[2]Departments of Medicine and Endocrinology, Austin Health, University of Melbourne, Melbourne, Australia
[3]Department of Community Medicine, UiT The Arctic University of Norway, Tromsø, Norway
[4]Department of Orthopaedic Surgery, University Hospital of North Norway, Tromsø, Norway
[5]Centre for Epidemiology and Biostatistics, School of Population and Global Health, University of Melbourne, Melbourne, Australia
[6]Department of Endocrinology, Morbid Obesity and Preventive Medicine, Oslo University Hospital, Oslo, Norway
[7]Department of Clinical Medicine, University of Oslo, Oslo, Norway
[8]Hudson Institute for Medical Research, Monash University, Melbourne, Australia
[9]Mary MacKillop Institute for Health Research, Australian Catholic University, Melbourne, Australia
[10]Department of Clinical Medicine, UiT The Arctic University of Norway, Tromsø, Norway
[11]Department of Obstetrics and Gynecology, University Hospital of North Norway, Tromsø, Norway

ABSTRACT

Advancing age is accompanied by a reduction in bone formation and remodeling imbalance, which produces microstructural deterioration. This may be partly caused by a diversion of mesenchymal cells towards adipocytes rather than osteoblast lineage cells. We hypothesized that microstructural deterioration would be associated with an increased marrow adiposity, and each of these traits would be independently associated with nonvertebral fractures and improve discrimination of women with fractures from controls over that achieved by femoral neck (FN) areal bone mineral density (aBMD) alone. The marrow adiposity and bone microstructure were quantified from HR-pQCT images of the distal tibia and distal radius in 77 women aged 40 to 70 years with a recent nonvertebral fracture and 226 controls in Melbourne, Australia. Marrow fat measurement from HR-pQCT images was validated using direct histologic measurement as the gold standard, at the distal radius of 15 sheep, with an agreement ($R^2 = 0.86$, $p < 0.0001$). Each SD higher distal tibia marrow adiposity was associated with 0.33 SD higher cortical porosity, and 0.60 SD fewer, 0.24 SD thinner, and 0.72 SD more-separated trabeculae (all $p < 0.05$). Adjusted for age and FN aBMD, odds ratios (ORs) (95% CI) for fracture per SD higher marrow adiposity and cortical porosity were OR, 3.39 (95% CI, 2.14 to 5.38) and OR, 1.79 (95% CI, 1.14 to 2.80), respectively. Discrimination of women with fracture from controls improved when cortical porosity was added to FN aBMD and age (area under the receiver-operating characteristic curve [AUC] 0.778 versus 0.751, $p = 0.006$) or marrow adiposity was added to FN aBMD and age (AUC 0.825 versus 0.751, $p = 0.002$). The model including FN aBMD, age, cortical porosity, trabecular thickness, and marrow adiposity had an AUC = 0.888. Results were similar for the distal radius. Whether marrow adiposity and cortical porosity indices improve the identification of women at risk for fractures requires validation in prospective studies. © 2019 American Society for Bone and Mineral Research.

KEY WORDS: CORTICAL POROSITY; HR-PQCT; MARROW ADIPOSITY; NONVERTEBRAL FRACTURE; WOMEN

Introduction

Ageing is associated with the development of abnormalities in bone remodeling.[1] Around midlife in women, remodeling becomes unbalanced and rapid. Less bone is deposited than resorbed by each remodeling event, resulting in microstructural deterioration. Porosity increases; cortices thin and become fragmented; and trabeculae thin, perforate, and

Received in original form December 30, 2017; revised form February 24, 2019; accepted March 1, 2019. Accepted manuscript online June 17, 2019.
Address correspondence to: Roger Zebaze, MD, Department of Medicine, School of Clinical Sciences, Monash Health, Monash University, 246 Clayton Rd, Clayton, VIC 3168, Australia. E-mail: Roger.Zebaze@monash.edu
*RZ and MO contributed equally to this work.
Journal of Bone and Mineral Research, Vol. 34, No. 8, August 2019, pp. 1451–1460
DOI: 10.1002/jbmr.3721

may eventually disappear.[2–5] Unbalanced remodeling upon the endocortical surface erodes the cortex and increases the medullary compartment volume, which in turn becomes occupied by fat cells, nonfat cells, and extracellular water.

The mechanisms responsible for the reduction in the volume of bone deposited by each remodeling event are unclear. However, osteoblasts and adipocytes share common precursor cells in the bone marrow, and decreased bone formation may be partly the result of enhanced adipogenesis in favor of osteoblastogenesis.[6–10]

There is an age-related increase in marrow adiposity and a reciprocal reduction in trabecular bone volume.[11–14] We propose that the proportions of this nonmineral compartment can be distinguished because fat cells attenuate photons less than the attenuation produced by water and nonfat cells.[15,16] Accordingly, we validated a method for identifying marrow adipose tissue from HR-pQCT images and we estimated a marrow adiposity index (MAI).

Combining microstructural deterioration with areal bone mineral density (aBMD) and Fracture Risk Assessment Tool (FRAX) results leaves more than half of the women with fractures unidentified.[17] We hypothesized that a higher MAI would be associated with microstructural deterioration and contribute to fracture risk independently of cortical porosity, and that both MAI and cortical porosity would improve discrimination of women with fractures from controls when added to FN aBMD.

Materials and Methods

Validation of marrow fat assessment using HR-pQCT with histology as gold standard

It has been shown, using histologic assessment as the gold standard, that dual energy computed tomography (DECT) can be used to accurately measure marrow fat.[18] We determined whether marrow fat could be accurately measured from images acquired using HR-pQCT and analyzed using StrAx software (StraxCorp, Melbourne, Australia), with coregistered histologic examinations as the gold standard. Twenty fresh sheep radii specimens were collected and stored at −20°C. Sheep are commonly used as an animal model for research in bone diseases because their bone architecture is similar to that of humans.[19] Specimens were sectioned at a 1.5-cm location proximal to the sheep wrist joint. The proximal part was sealed to avoid any loss of fat or bone tissue and scanned using HR-pQCT. After HR-pQCT imaging, proximal parts were cut and a 1-cm-thick section was kept. These sections were decalcified. The sections were cut into left and right halves to fit the field of view of the microscope for histologic imaging. Each half was embedded in paraffin wax and stained with H&E. The scanning protocol ensured that the first HR-pQCT slice corresponded to the histologic section in which marrow fat was measured. The process of coregistration of the histologic cross-sections with HR-pQCT imaging and an example of adipose tissue seen after H&E staining is shown in Fig. 1.

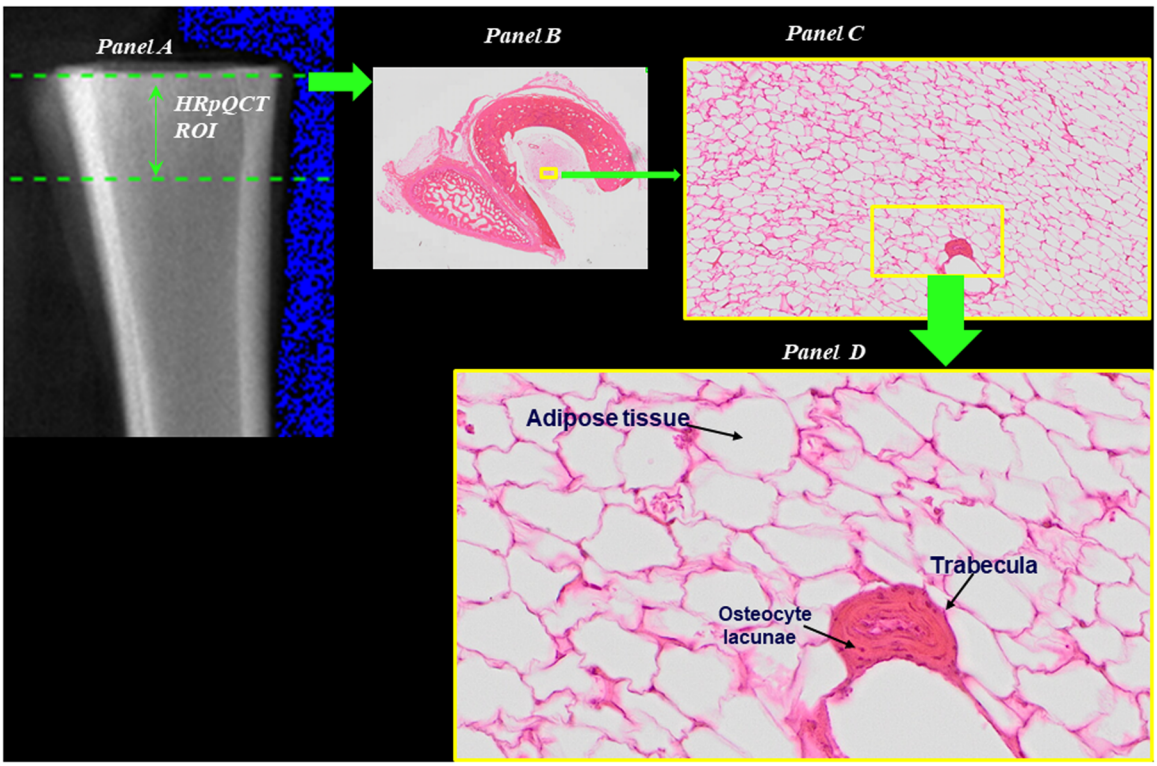

Fig. 1. Coregistration between histologic examination versus HR-pQCT imaging; and marrow fat after H&E staining. (Panel *A*) Scout view of a sheep radius and an example of ROI placement. The first slice of the HR-pQCT image corresponds to the histologic cross-section. (Panel *B*) Half of the cross-section after decalcification and H&E staining. The compact-cortex and the marrow cavity are visible. A distinct adjacent ulna (smaller bone) is also visible. (Panel *C*) A magnified view of an area within the marrow cavity shows adipose tissue cells, which appear as empty spaces. This is caused by the extraction of fat during processing. (Panel *D*) A further magnification of the same area shows adipose tissue more clearly. A cross-section of a trabecula with osteocytes lacunae is also discernible.

HR-pQCT imaging and marrow fat measurement

One-hundred ten HR-pQCT slices were obtained from the distal end of sheep radii. They were scanned moving proximally, as per the manufacturer's protocol, to collect HR-pQCT images in vivo. An Xtreme CT II (Scanco Medical AG, Brüttisellen, Switzerland) was used, but with an XtremeCT I-equivalent protocol. Images were analyzed using StrAx software. The proportion of fat voxels within the marrow cavity—adipose volume (AV) to total marrow volume (TV) was outputted.

Histological imaging and marrow fat measurement

A full digital image of each half cross-section was captured using an Olympus VS120 microscope (Olympus Corp., Tokyo, Japan) with a color camera at 20× magnification. The images were analyzed using ImageJ.[20] In brief, the scale was calibrated to 512 pixels/mm and the images were converted to an 8-bit gray scale. The trabecular compartment in each cross-sectional half was segmented. Areas in the marrow cavity occupied by adipocyte tissue were identified as void spaces remaining from the H&E staining. Areas with artifacts were avoided during the quantification process. AV/TV was calculated for each half. After excluding 5 of the 20 samples with artifacts such as folding during preparation, the analysis was restricted to the remaining 15 samples.

Subjects

We recruited 84 women above 40 years of age within 14 days of having had a nonvertebral fracture to minimize the likelihood that changes in cortical porosity or medullary composition followed the fracture (Fig. 2). These women presented to the Emergency Department at Austin Health, Melbourne, Australia. The 84 women had a fracture at the distal forearm ($n = 52$), upper arm ($n = 5$), elbow ($n = 5$), hand ($n = 2$), rib ($n = 1$), hip ($n = 3$), lower leg ($n = 6$), ankle ($n = 9$), or toe ($n = 1$). After excluding 5 women receiving hormone replacement therapy (HRT), and 2 and 10 women with movement artifact during image acquisition of the distal tibia and the distal radius, respectively, 77 and 69 women with a fracture remained with valid measurements of the distal tibia and the distal radius, respectively.

We compared the measurements with those of healthy twins from the Twins Research Australia ($n = 653$).[3,21,22] Among these controls, we excluded 30 women taking HRT, 108 women below 40 years of age, 170 women with a prior fracture, 11 and 37 women with movement artifacts of the distal tibia and the distal radius, respectively, leaving 334 and 308 controls with valid measurements of the distal tibia and the distal radius, respectively. Of the 334 controls with valid measurements of the distal tibia, 118 were singletons and 216 were twins. We randomly selected one twin from each pair ($n = 108$), and $118 + 108 = 226$ singletons were left included as controls in the analysis of distal tibia measurements. Of the 308 controls with valid measurements of the distal radius, 120 were singletons and 188 were twins. We randomly selected one twin for each pair ($n = 94$), and $120 + 94 = 214$ singletons were left included as controls in the analysis of distal radius measurements.

The participants answered a questionnaire including information on their prior fracture, diseases, use of medication, menstruation, menopause, and lifestyle, including weekly hours they participated in light (walking, lawn bowls, light gardening), moderate (social tennis, golf, hiking), or vigorous physical activity (competitive active sports). A physical activity

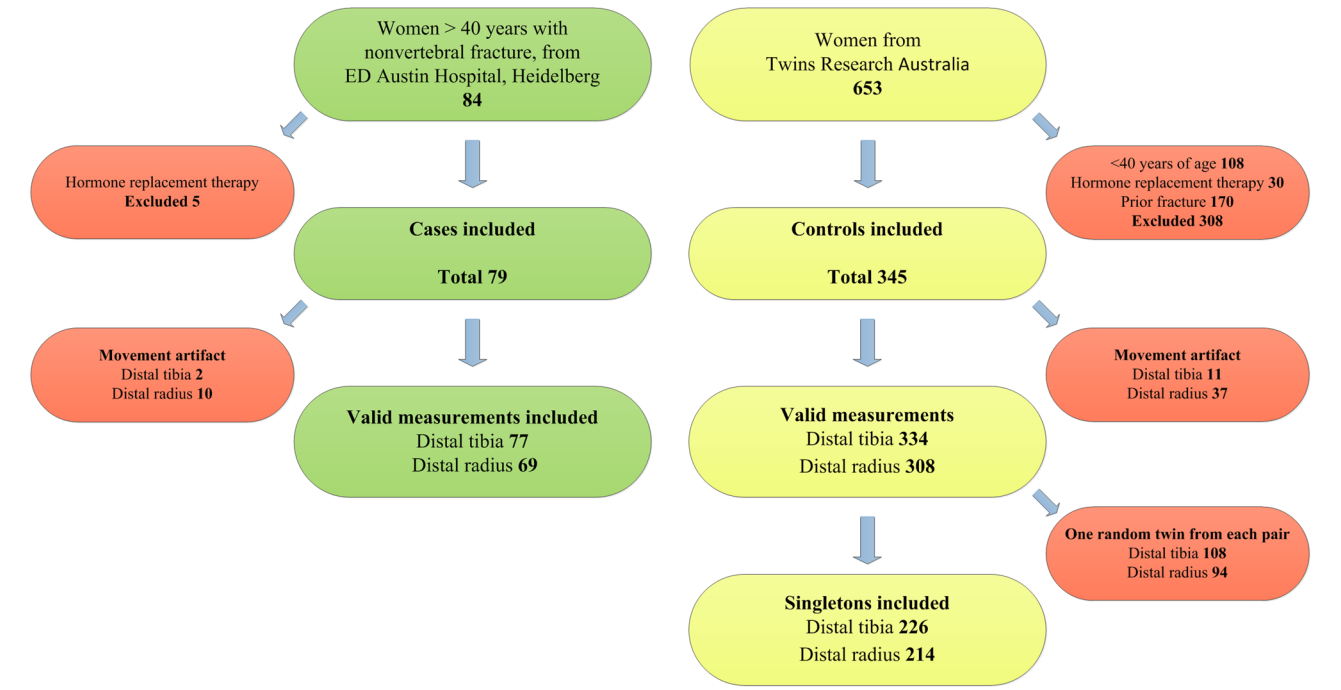

Fig. 2. Participants in the case-control study from 2008 to 2012.

index was made by adding hours of light, moderate, and vigorous activity, giving the hours with moderate and vigorous physical activity double and triple weight: index = light + 2 moderate + 3vigorous. Women were classified as postmenopausal (amenorrhea for more than 1 year), perimenopausal (no cycles for 3 to 12 months), and premenopausal (a regular cycle in the last 3 months). All women gave written informed consent. The Austin Health Human Research Ethics Committee approved the study.

Measurements

Height and weight were measured while wearing light clothing and no shoes. HR-pQCT (XtremeCT, isotropic resolution of 82 μm) was used to obtain images at the nondominant distal tibia and distal radius.[23] In those with fracture at the nondominant side, the opposite side was scanned. The 110 CT slices were obtained at a standardized distance of 22.5 and 9.5 mm from a reference line that was manually placed at the endplate of the distal tibia and distal radius, respectively. The 49 most proximal slices in 110 slices of the region of interest were chosen because the thicker cortex allows an accurate assessment of cortical porosity.[21,22,24]

Cortical and trabecular morphology and a MAI, a surrogate of marrow fat, were quantified using StrAx software, a nonthreshold-based method that selects attenuation profile curves and segments the bone into the compact-appearing cortex, outer (OTZ) and inner transitional zones (ITZ), and the trabecular compartment.[25] Local bone edges were identified as the beginning and the end of the rising and falling S-shaped portions of the profile curve enabling the delineation of the compartments. The density profile curve produced had two plateaus: one corresponding to the compact-appearing cortex and one corresponding to the trabecular compartment. Between these plateaus was a descending S-shaped curve or transition between the two plateaus. This was the transitional zone.[25] The porosity quantified by the StrAx algorithm is the proportion of void within each voxel. This method confined cortical porosity and cortical fragments to the transitional zone, and not to the medullary canal yielding a higher cortical porosity than reported using threshold-based methods.[25,26] The precision of the measurements had coefficients of variation (CV) < 4%.[25] Trabecular number, thickness, separation, trabecular bone volume per tissue volume (BV/TV), and volumetric BMD (vBMD) were also quantified using the StrAx software.

The medullary canal contains fat cells, mineralized matrix, nonfat cells, and water. Voxels containing fat cells can be identified because their photons attenuation is below that of water. Thus, in HR-pQCT images, adipose volume (AV) was defined as the total volume of the marrow cavity (TV) occupied by voxels with attenuation below that of water. We expressed the fat proportion (FP) = 100 * AV/TV (%). As age-related endocortical resorption increases the medullary cavity, this reduces the fat proportion, but not the nonmineral apparent density produced by the fat cells, nonfat cells, and water. We calculated a relative medullary density (RMD) as a percentage of fully mineralized bone matrix (1200 mg HA/cm^3). As the RMD decreases as fat cells increase, we subtracted this value from 100 for ease of comprehension, and RMD $(\%) = 100 - \left[100 * \frac{\text{Mean Medullary Density}}{1200}\right]$ (Fig. 3). The MAI is a function of the fat proportion and the relative medullary density, $\text{MAI} = \frac{\text{FP} * \text{RMD}}{100}$. As we did not measure the absolute content of fat cells in the medullary cavity, we refer to the MAI as an indicator of the presence of fat cells.

FN aBMD was assessed using DXA (Lunar Prodigy, Lunar Corp., Madison, WI, USA) at the left femur, and CV was 2.6%. The women were categorized into those with normal FN aBMD (*T*-score >−1.0), osteopenia (*T*-score between −2.5 and −1.0) and osteoporosis (*T*-score <−2.5) using the World Health Organization's classification.[27]

Statistical analyses

To validate StrAx software quantification of marrow fat in sheep radii, linear regression was used to determine the R^2 between the gold standard and StrAx measurements. The root mean square error (RMSE) between StrAx measurement and the gold standard was quantified. A Bland-Altman plot was used to assess the difference between the two measurement methods.

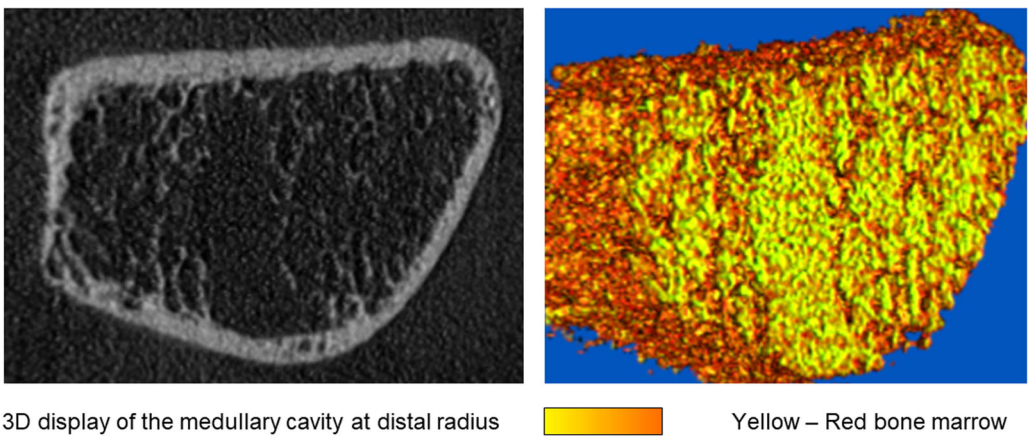

Fig. 3. HR-pQCT images of a human distal radius showing voxels in the marrow cavity that are color-coded in a scale ranging from red to yellow depending on their attenuation relative to water. The larger the proportion of yellow bone marrow (fat cells) versus red bone marrow (hematopoietic cells), the lower is the density.

In women, summary statistics are presented as mean and SD. We compared the distal tibia and distal radius parameters in cases and controls, taking into account the menopausal status, physical activity, and age, using a semiparametric regression model. We used fracture status, menopausal status, and physical activity as parametric variables and age as a nonparametric variable because age had a nonlinear relationship with bone parameters, with almost no change from 40 until approximately 47 years of age. Menopausal status alone was associated with bone parameters before, but not after adjustment for age. The semiparametric regression models were also used to assess the associations of cortical and trabecular morphology as a function of the marrow adiposity index, adjusted for height, weight, physical activity, and fracture status (when significant) as parametric variables, and age as a nonparametric variable. Coefficients and SEs with three decimals, exact p values, and R-square are presented together to illustrate which of the variables are most strongly associated.

Odds ratio (OR) for fracture per 1 SD change in cortical porosity, MAI, and other cortical and trabecular bone morphology were calculated in logistic regression analyses adjusted for age (quadratic model) and FN aBMD. Distal tibia and distal radius variables were standardized to have mean = 0 and SD = 1 in the linear and logistic regression analysis. In final multivariable models, we combined cortical porosity and MAI in the same models, adjusted for age, FN aBMD, and covariates that were the best subsets of variables.[28] We calculated area under the receiver operating characteristic curve (AUC) using logistic regression analysis to determine whether discrimination of women with fractures from controls was improved when adding microstructure and MAI to the reference model 1 (age, age^2, and FN aBMD), and the reference model 2 (age, age^2, FN aBMD, and MAI). The final models were also adjusted for significant covariates. Chi-square p value was used to compare the AUC after additional adjustment for covariates. Analyses were performed using STATA Software package, v14 (StataCorp, College Station, TX, USA) and SAS software package, v9.4 (SAS Institute Inc., Cary, NC, USA). All tests were two-sided and $p < 0.05$ was considered significant.

Results

Accuracy of the marrow fat measurement in sheep radii

AV/TV measured from HR-pQCT images using StrAx predicted the gold-standard histologic measurement of marrow with an R^2 of 0.86 ($p < 0.001$) and a RMSE of 0.96% (Fig. 4). Bland-Altman plot showed that HR-pQCT overestimated AV/TV by on average 2.67% ± 1.00% ($p < 0.001$).

Marrow adiposity index is associated with microstructure

Fracture cases had higher distal tibial MAI, higher porosity, and lower trabecular BV/TV and FN aBMD than controls, adjusted for menopausal status, physical activity, and age (all $p < 0.01$; Table 1). Each SD higher MAI was associated with 0.14, 0.17, and 0.80 SD higher porosity of the compact-appearing cortex, and outer and inner transitional zones, respectively; 0.16 SD thinner cortices; 0.60 SD lower trabecular number; and 0.24 SD thinner and 0.72 SD more-separated trabeculae (all $p \le 0.01$; Table 2). MAI explained 5% to 66% of the variance in cortical and 10% to 86% of the variance in trabecular parameters. All results were adjusted for age, fracture status, physical activity, height, and weight. Results were similar for the distal radius as shown in Tables 1 and 2.

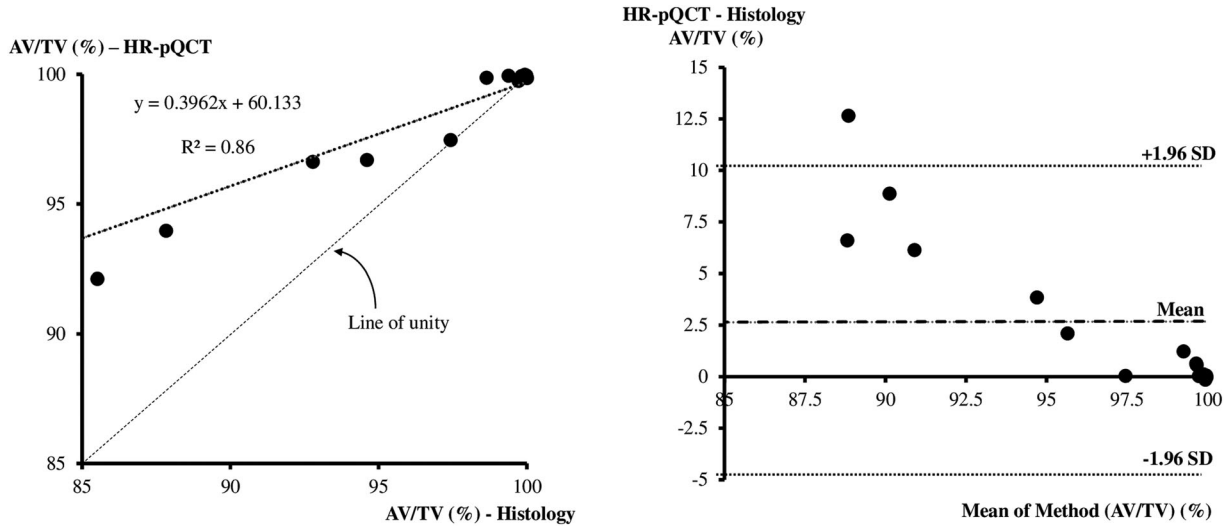

Fig. 4. (Left) Correlation of adipose volume (AV) to total marrow volume (TV) (expressed as a percentage) as measured using HR-pQCT versus histology (gold standard). (Right) This is the corresponding Bland-Altman plot.

Table 1. Characteristics of Women by Fracture Status

	Cases $n = 77$	Controls $n = 226$	p
Age (years)	54.3 ± 6.4	51.0 ± 8.7	0.002
Height (cm)	162.7 ± 6.5	162.9 ± 6.4	0.818
Weight (kg)	72.3 ± 14.2	70.8 ± 15.5	0.432
Light physical activity (hours/week)	5.0 ± 4.5	4.9 ± 3.5	0.863
Moderate physical activity (hours/week)	1.5 ± 3.3	1.1 ± 2.0	0.091
Vigorous physical activity (hours/week)	0.8 ± 2.2	0.8 ± 1.6	0.109
Physical activity index	10.1 ± 11.1	9.5 ± 7.4	0.551
Premenopausal women, *n* (%)	11 (14.3)	156 (57.5)	<0.001
Perimenopausal women, *n* (%)	10 (13.0)	21 (9.3)	0.355
Postmenopausal women, *n* (%)	56 (72.7)	75 (33.3)	<0.001
Femoral neck (FN) aBMD (mg/cm^2)	0.89 ± 0.12	0.98 ± 0.15	<0.001
FN normal aBMD, *n* (%)	44 (57.9)	175 (78.5)	<0.001
FN osteopenia, *n* (%)	31 (40.8)	44 (19.7)	<0.001
FN osteoporosis, *n* (%)	1 (1.3)	4 (1.8)	0.780
Distal Tibia	$n = 77$	$n = 226$	
Total cortical porosity (%)	64.5 ± 5.8	60.0 ± 6.2	7.7×10^{-7}
Compact cortex porosity (%)	46.7 ± 7.4	42.1 ± 7.2	0.0001
Outer transitional zone porosity (%)	47.5 ± 6.6	43.1 ± 6.2	1.4×10^{-6}
Inner transitional zone porosity (%)	87.1 ± 3.2	84.7 ± 3.2	9.7×10^{-6}
Cortical thickness (mm)	2.36 ± 0.31	2.34 ± 0.24	0.157
Trabecular number (1/mm)	2.15 ± 0.51	2.76 ± 0.66	3.3×10^{-11}
Trabecular thickness (mm)	0.20 ± 0.01	0.19 ± 0.01	1.1×10^{-5}
Trabecular separation (mm)	1.58 ± 0.31	1.32 ± 0.29	3.2×10^{-8}
Trabecular bone volume/tissue volume (%)	2.93 ± 1.46	4.13 ± 1.73	2.2×10^{-6}
Trabecular volumetric BMD (mg HA/cm^3)	111 ± 40.5	131 ± 41.1	0.003
Marrow adiposity index	43.5 ± 3.2	39.9 ± 3.9	5.5×10^{-12}
Distal Radius	$n = 69$	$n = 214$	
Total cortical porosity (%)	57.8 ± 5.3	53.7 ± 6.1	1.7×10^{-6}
Compact cortex porosity (%)	40.4 ± 5.3	36.5 ± 5.6	1.2×10^{-6}
Outer transitional zone porosity (%)	43.6 ± 4.9	40.0 ± 4.9	3.7×10^{-8}
Inner transitional zone porosity (%)	86.9 ± 2.7	84.5 ± 2.9	3.1×10^{-6}
Cortical thickness (mm)	1.82 ± 0.19	1.81 ± 0.20	0.870
Trabecular number (1/mm)	1.88 ± 0.55	2.34 ± 0.51	3.0×10^{-8}
Trabecular thickness (mm)	0.20 ± 0.01	0.19 ± 0.01	3.2×10^{-5}
Trabecular separation (mm)	1.65 ± 0.36	1.36 ± 0.30	6.2×10^{-7}
Trabecular bone volume/tissue volume (%)	1.84 ± 1.14	3.04 ± 1.57	3.6×10^{-6}
Trabecular volumetric BMD (mg HA/cm^3)	98.3 ± 41.5	122 ± 43.0	0.009
Marrow adiposity index	48.3 ± 3.4	44.0 ± 4.3	2.4×10^{-11}

Numbers are mean ± standard deviation, or number (%). aBMD = areal bone mineral density.

Cases and controls were compared using semi-parametric regression, adjusted for menopausal status and physical activity as parametric components and age as a non-parametric component.

Marrow adiposity index and cortical porosity improved discrimination of fractures

Each SD increment in MAI of distal tibia was associated with fractures adjusted for age, FN aBMD, and cortical porosity (OR, 3.39, 95% CI, 2.14 to 5.38; Table 3). Each SD higher cortical porosity was associated with fractures adjusted for age, FN aBMD, and MAI (OR, 1.79, 95% CI, 1.14 to 2.80). There were no interactions between MAI, FN aBMD, or cortical porosity. The discrimination of women with fractures from controls was improved when distal tibia cortical porosity was added to FN aBMD and age (AUC 0.778 versus 0.751, $p = 0.006$) or MAI was added to FN aBMD and age (AUC 0.825 versus 0.751, $p = 0.002$; Table 4). The model including distal tibia cortical porosity, trabecular thickness, MAI, FN aBMD, age, and weight had an AUC = 0.888. Results were similar for the distal radius as shown in Tables 3 and 4.

Discussion

We report that marrow fat can be accurately measured from the analysis of HR-pQCT images acquired in vivo in clinical and research settings. We further extended these findings by showing that marrow fat so measured can be used to produce a MAI that improves the identification of women with nonvertebral fractures and does so independently of other metrics such as cortical porosity and FN aBMD.

Table 2. Association of a 1 SD Increment in Marrow Adiposity Index (Predictor) with Each Cortical and Trabecular Trait of Distal Tibia and Distal Radius (Outcomes)

	Distal tibia				Distal radius			
Outcome variables	Coefficient	SE	*p*	R^2	Coefficient	SE	*p*	R^2
Total cortical porosity (%)	0.334	0.042	2.9×10^{-14}	0.32	0.340	0.050	9.6×10^{-11}	0.29
Compact cortex porosity (%)	0.136	0.043	0.002	0.20	0.168	0.050	0.001	0.19
Outer transitional zone porosity (%)	0.170	0.042	6.8×10^{-5}	0.19	0.205	0.045	8.0×10^{-6}	0.20
Inner transitional zone porosity (%)	0.797	0.035	8.1×10^{-68}	0.66	0.772	0.034	7.8×10^{-65}	0.64
Cortical thickness (mm)	−0.161	0.064	0.012	0.05	−0.058	0.061	0.348	0.003
Trabecular number (1/mm) – linear	−0.601	0.041	9.7×10^{-38}	0.59	−0.700	0.040	6.5×10^{-47}	0.53
Trabecular thickness (mm)	−0.244	0.062	9.4×10^{-5}	0.10	−0.284	0.058	1.6×10^{-6}	0.13
Trabecular separation (mm) – linear	0.723	0.039	3.9×10^{-51}	0.64	0.782	0.035	2.2×10^{-64}	0.64
Trabecular BV/TV (%) – linear	−3.023	0.310	1.2×10^{-19}	0.86	−3.395	0.291	6.1×10^{-26}	0.89
– quadratic	2.084	0.312	1.2×10^{-10}		2.464	0.293	2.1×10^{-15}	
Trabecular vBMD (mg HA/cm^3) – linear	−2.542	0.521	1.7×10^{-6}	0.61	−2.886	0.521	7.0×10^{-8}	0.64
– quadratic	1.770	0.522	0.001		2.084	0.525	9.2×10^{-5}	

Coefficient = standardised regression coefficient; SE = standard error; R^2 = Adjusted coefficient of determination (R-square).

Semi-parametric regression model was fitted to the data, adjusted for height, weight, physical activity and fracture status whenever significant as parametric components and age as non-parametric component.

Historically, the clinical assessment of marrow adiposity required a bone biopsy. Recently, with advances in imaging techniques, there is increasing evidence that the role of marrow adiposity on skeletal health can be studied directly and noninvasively. Until recently, the noninvasive assessment of marrow fat has been limited to MRI. However, MRI is not readily available for the purpose of quantifying marrow fat, and is costly. Thus, there is a need to develop more readily available, inexpensive, and rapid approaches to quantify bone marrow fat in in vivo settings. It has been reported that marrow fat measured from histologic images processed after H&E staining agreed with marrow fat quantified using in vivo imaging modalities: DECT and MRI.[25] There are also studies showing that single energy high resolution-QCT can be used to measure marrow fat.[29] In this study, we complemented these findings by showing that marrow fat measured from HR-pQCT images showed an excellent correlation with marrow fat measured from histologic images after H&E staining.

Most fragility fractures occur in women with osteopenia or normal aBMD, not women with osteoporosis.[30] High vertebral marrow adiposity is associated with vertebral fracture independent of aBMD.[13,31] Vertebral marrow adiposity is 10% and 5% higher in patients with osteoporosis and osteopenia without fracture, respectively, compared to age-matched healthy controls,[15,31–34] suggesting an association between marrow adiposity and aBMD.[15] We found that the distal tibia MAI, together with cortical porosity and trabecular thickness best discriminated women with fracture from controls, and did so independent of FN aBMD and age. Another study has reported that a combination of cortical and trabecular microstructure improved fracture prediction.[35]

Marrow adiposity was associated with porosity of each cortical compartment, particularly of the inner transitional zone adjacent to the medullary cavity. However, the association between the MAI and the porosity of the compact cortex, located more distant from the marrow cavity, is likely to be more important in compromising bending strength.[36] The MAI was also associated with fewer, thinner more-separated trabeculae, and lower trabecular BV/TV and vBMD. Nevertheless, the MAI was associated with fracture prevalence independently of cortical and trabecular microstructure. We also took into account height, weight, physical activity, and the menopausal status in the analysis of this study; however, when the effect of age was taken into account, the menopausal status made no additional contribution to the association between bone and fat traits.

The reasons for the association of the MAI with deteriorated microstructure and the improved discrimination of fractures independently of bone microstructure are unclear. There may be a shift from osteogenesis to adipogenesis, remodeling imbalance, leading to reduced bone strength, and thus an increase in fracture risk.[10,37]

Low estrogen levels after menopause may contribute to increased adipogenesis, as estrogen treatment of osteoporotic postmenopausal women prevented an increase in marrow adiposity compared with controls treated with placebo.[10,38] In the only study that we are aware of using pQCT for quantification of marrow cavity fat, loading was associated with lower marrow fat, which in turn was associated with greater bone strength, larger midtibial cortical area—not cortical vBMD.[39] In a study using MRI, runners had lower lumbar vertebral marrow fat fraction than nonsporting controls, suggesting that exercise may reduce the age-related increase in marrow adiposity.[40]

This study has several limitations. As it was cross-sectional, we could not assess causation between marrow adiposity, microstructure, and fracture. From HR-pQCT images, we assessed voxels within the marrow cavity not occupied by bone. The other components of those voxels are fat cells and nonfat content such as other cells and water. As we did not measure the absolute content of fat cells in the marrow cavity, we refer to a MAI, an indicator of the presence of fat cells. Nevertheless, marrow fat measured from HR-pQCT images and directly from histologic images showed agreement. As compared to histologic measurements, HR-pQCT overestimated marrow fat with a bias by on average 2.67%. This bias can be explained by a partial volume effect resulting from voxels containing marrow fat; mineralized bone matrix at the edge between trabeculae and marrow fat are classified as fat voxels in HR-pQCT images. Increased marrow adiposity can result in considerable measurement errors in aBMD,[41,42] and may have

confounded the associations observed in the current study to some extent.

In summary, marrow fat can be accurately measured from HR-pQCT images and used in vivo to provide a MAI. A higher MAI was associated with microstructural deterioration and the presence of nonvertebral fractures independent of this microstructural deterioration and FN aBMD. Discrimination of fracture cases from controls may be improved when marrow adiposity and cortical porosity are combined with FN aBMD. Prospective studies are needed to validate these observations.

Disclosures

RZ has received grant and/or research support from Amgen, AKP, GSK, and Pfizer. He is a shareholder and a director on the board of StraxCorp. AG-Z is remunerated by StraxCorp as a senior image analyst. ES has received research support and has lectured at meeting symposia funded by Amgen, Allergan, and Asahi. He is a director of the board and shareholder in StraxCorp. EFE is a member of the advisory board for Amgen, MSD, Novartis, and Lilly and has received consulting fees from IDS and speaker fees from Amgen, MSD,

Table 3. Fracture Risk by 1 Standard Deviation (SD) Increment in Cortical and Trabecular Bone Morphology of Distal Tibia and Distal Radius

	Odds Ratio (95% CI)	*p*
Unadjusted analysis		
Age (years) – linear	3.03 (1.88–4.87)	7.1×10^{-6}
– quadratic	0.99 (0.986–0.995)	1.7×10^{-5}
Height (cm)	1.00 (0.96–1.04)	0.830
Weight (kg)	1.01 (0.99–1.02)	0.427
Physical activity (hours/week)	1.01 (0.98–1.04)	0.550
Femoral neck (FN) aBMD (mg/cm^2)	0.52 (0.38–0.70)	2.4×10^{-5}
Distal Tibia		
Adjusted for age (quadratic) and FN aBMD		
Total cortical porosity (%)	2.31 (1.53–3.49)	8.7×10^{-5}
Compact cortex porosity (%)	1.90 (1.28–2.81)	0.002
Outer transitional zone porosity (%)	2.22 (1.46–3.36)	2.1×10^{-4}
Inner transitional zone porosity (%)	2.05 (1.34–3.14)	0.001
Cortical thickness (mm)	1.37 (1.03–1.83)	0.033
Trabecular number (1/mm)	0.29 (0.19–0.46)	1.5×10^{-7}
Trabecular thickness (mm)	2.04 (1.50–2.77)	8.5×10^{-6}
Trabecular separation (mm)	2.35 (1.59–3.47)	2.3×10^{-5}
Trabecular bone volume/tissue volume (%)	0.41 (0.26–0.64)	1.4×10^{-4}
Trabecular volumetric BMD (mg HA/cm^3)	0.76 (0.53–1.11)	0.158
Marrow adiposity index	3.84 (2.44–6.04)	1.5×10^{-8}
Additional analysis adjusted for all covariates in multivariable models[a]		
Total cortical porosity (%)	2.62 (1.50–4.58)	0.001
Cortical thickness (mm)	1.56 (1.08–2.28)	0.019
Trabecular thickness (mm)	2.30 (1.61–3.29)	9.7×10^{-6}
Marrow adiposity index	3.60 (2.20–5.90)	8.2×10^{-7}
Distal Radius		
Adjusted for age (quadratic) and FN aBMD		
Total cortical porosity (%)	2.12 (1.48–3.05)	6.0×10^{-5}
Compact cortex porosity (%)	2.21 (1.52–3.21)	4.3×10^{-5}
Outer transitional zone porosity (%)	2.53 (1.67–3.84)	1.9×10^{-5}
Inner transitional zone porosity (%)	2.34 (1.54–3.55)	8.1×10^{-5}
Cortical thickness (mm)	1.11 (0.83–1.49)	0.476
Trabecular number (1/mm)	0.37 (0.25–0.57)	6.1×10^{-6}
Trabecular thickness (mm)	1.95 (1.40–2.70)	9.0×10^{-5}
Trabecular separation (mm)	2.21 (1.51–3.23)	6.1×10^{-5}
Trabecular bone volume/tissue volume (%)	0.35 (0.22–0.57)	3.4×10^{-5}
Trabecular volumetric BMD (mg HA/cm^3)	0.71 (0.49–1.03)	0.072
Marrow adiposity index	4.35 (2.67–7.10)	1.1×10^{-8}
Additional analysis adjusted for all covariates in multivariable models[a]		
Total cortical porosity (%)	1.53 (0.99–2.37)	0.054
Trabecular thickness (mm)	2.50 (1.71–3.65)	3.6×10^{-6}
Marrow adiposity index	4.25 (2.50–7.22)	1.9×10^{-7}

[a]The multivariable logistic regression models were adjusted for age, FN aBMD and all significant covariates. Distal tibia and distal radius variables were standardised to have mean = 0 and SD = 1.

Table 4. Area Under the Receiver Operating Characteristic Curve (AUC) for the Reference Model and the Incremental Contribution of Cortical and Trabecular Bone Morphology of Distal Tibia and Distal Radius to Prediction of Fracture

	AUC	95% CI	Change in AUC	*p*
Distal Tibia				
Reference model 1: age, age^2 and FN aBMD	0.751	0.69-0.81		
Total cortical porosity (%)	0.796	0.74-0.85	**0.045**	**0.006**[a]
Compact cortex porosity (%)	0.778	0.72-0.84	**0.028**	**0.039**[a]
Outer transitional zone porosity (%)	0.794	0.74-0.85	**0.043**	**0.007**[a]
Inner transitional zone porosity (%)	0.776	0.71-0.84	0.025	0.119[a]
Cortical thickness (mm)	0.758	0.70-0.82	0.007	0.556[a]
Trabecular number (1/mm)	0.825	0.77-0.88	**0.074**	**0.0002**[a]
Trabecular thickness (mm)	0.790	0.73-0.85	**0.040**	**0.034**[a]
Trabecular separation (mm)	0.798	0.74-0.85	**0.048**	**0.009**[a]
Trabecular bone volume/tissue volume (%)	0.787	0.73-0.85	0.037	0.060[a]
Trabecular volumetric BMD (mg HA/cm^3)	0.755	0.69-0.82	0.004	0.594[a]
Marrow adiposity index (MAI)	0.825	0.77-0.88	**0.075**	**0.002**[a]
Reference model 2: age, age^2, FN aBMD and MAI	0.825	0.77-0.88		
Total cortical porosity (%)	0.843	0.79-0.89	**0.017**	**0.049**[b]
Trabecular number (1/mm)	0.847	0.80-0.89	**0.022**	**0.023**[b]
Trabecular thickness (mm)	0.870	0.83-0.91	**0.044**	**0.007**[b]
Distal Radius				
Reference model 1: age, age^2 and FN aBMD	0.742	0.68-0.81		
Total cortical porosity (%)	0.788	0.73-0.85	**0.047**	**0.013**[a]
Compact cortex porosity (%)	0.791	0.73-0.85	**0.050**	**0.010**[a]
Outer transitional zone porosity (%)	0.796	0.73-0.86	**0.054**	**0.007**[a]
Inner transitional zone porosity (%)	0.775	0.71-0.84	0.034	0.116[a]
Cortical thickness (mm)	0.742	0.68-0.81	0.001	0.889[a]
Trabecular number (1/mm)	0.772	0.73-0.85	**0.051**	**0.027**[a]
Trabecular thickness (mm)	0.775	0.71-0.84	0.034	0.119[a]
Trabecular separation (mm)	0.778	0.72-0.84	0.037	0.079[a]
Trabecular bone volume/tissue volume (%)	0.788	0.73-0.85	0.046	0.051[a]
Trabecular volumetric BMD (mg HA/cm^3)	0.745	0.68-0.81	0.003	0.764[a]
Marrow adiposity index (MAI)	0.833	0.78-0.89	**0.092**	**0.001**[a]
Reference model 2: age, age^2, FN aBMD and MAI	0.833	0.78-0.89		
Total cortical porosity (%)	0.840	0.79-0.89	0.006	0.311[b]
Trabecular number (1/mm)	0.835	0.78-0.89	0.001	0.797[b]
Trabecular thickness (mm)	0.882	0.84-0.93	**0.048**	**0.009**[b]

FN aBMD = femoral neck areal bone mineral density.
P-value for difference in AUC when compared to
[a]Reference model 1 and.
[b]Reference model 2.

Novartis, and Lilly. All authors state that they have no other conflicts of interest.

Acknowledgments

This study was funded by NHMRC (Project Grant ID: 1004938) and by the Research Council of Norway (RCN) Grant (ID 178588/V50). This study was facilitated by access to the Australian Twin Registry, a national resource supported by an Enabling Grant (ID 628911) from the National Health & Medical Research Council (NHMRC) of Australia. We thank Kylie King for her excellent contribution to the recruitment of the participants and data collection.

Authors' roles: Study design and conduct: MO, ÅB, EFE, RZ, ES. Data collection: ÅB, AGZ, XW. Responsibility for StrAx analysis: AGZ, RZ. Statistical analyses: MB, MO, ML, ÅB. MAI calculation: RZ. Marrow fat validation: RZ, AV, PE, CSL supervised by RZ. Drafting manuscript: all authors. Data interpretation and approving final version of manuscript: all authors. ÅB takes responsibility for the integrity of the data analysis.

References

1. Seeman E, Delmas PD. Bone quality—the material and structural basis of bone strength and fragility. N Engl J Med. 2006;354(21):2250–61.
2. Seeman E. Age-and menopause-related bone loss compromise cortical and trabecular microstructure. J Gerontol A Biol Sci Med Sci. 2013;68(10):1218–25.
3. Bjørnerem Å, Ghasem-Zadeh A, Bui M, et al. Remodeling markers are associated with larger intracortical surface area but smaller trabecular surface area: a twin study. Bone. 2011;49(6):1125–30.
4. Shigdel R, Osima M, Ahmed LA, et al. Bone turnover markers are associated with higher cortical porosity, thinner cortices, and larger size of the proximal femur and non-vertebral fractures. Bone. 2015;81:1–6.

5. Shigdel R, Osima M, Lukic M, et al. Determinants of transitional zone area and porosity of the proximal femur quantified in vivo in postmenopausal women. J Bone Miner Res. 2016;31(4): 758–66.
6. Moerman EJ, Teng K, Lipschitz DA, Lecka-Czernik B. Aging activates adipogenic and suppresses osteogenic programs in mesenchymal marrow stroma/stem cells: the role of PPAR-γ2 transcription factor and TGF-β/BMP signaling pathways. Aging Cell. 2004;3(6): 379–89.
7. Abdallah BM, Haack-Sørensen M, Fink T, Kassem M. Inhibition of osteoblast differentiation but not adipocyte differentiation of mesenchymal stem cells by sera obtained from aged females. Bone. 2006;39(1):181–8.
8. Song L, Liu M, Ono N, Bringhurst FR, Kronenberg HM, Guo J. Loss of wnt/β-catenin signaling causes cell fate shift of preosteoblasts from osteoblasts to adipocytes. J Bone Miner Res. 2012;27(11):2344–58.
9. Muruganandan S, Roman A, Sinal C. Adipocyte differentiation of bone marrow-derived mesenchymal stem cells: cross talk with the osteoblastogenic program. Cell Mol Life Sci. 2009;66(2):236–53.
10. Fazeli PK, Horowitz MC, MacDougald OA, Scheller EL, Rodeheffer MS, Rosen CJ, et al. Marrow fat and bone—new perspectives. J Clin Endocrinol Metab. 2013;98(3):935–45.
11. Rosen CJ, Bouxsein ML. Mechanisms of disease: is osteoporosis the obesity of bone? Nat Clin Pract Rheumatol. 2006;2(1):35–43.
12. Justesen J, Stenderup K, Ebbesen E, Mosekilde L, Steiniche T, Kassem M. Adipocyte tissue volume in bone marrow is increased with aging and in patients with osteoporosis. Biogerontology. 2001;2(3):165–71.
13. Schwartz AV, Sigurdsson S, Hue TF, et al. Vertebral bone marrow fat associated with lower trabecular BMD and prevalent vertebral fracture in older adults. J Clin Endocrinol Metab. 2013;98(6): 2294–300.
14. Devlin MJ, Rosen CJ. The bone–fat interface: basic and clinical implications of marrow adiposity. Lancet Diabetes Endocrinol. 2015;3(2):141–7.
15. Veldhuis-Vlug AG, Rosen CJ. Mechanisms of marrow adiposity and its implications for skeletal health. Metabolism. 2017;67:106–14.
16. Vogler J, 3rd, Murphy W. Bone marrow imaging. Radiology. 1988;168(3):679–93.
17. Ahmed LA, Shigdel R, Joakimsen R, et al. Measurement of cortical porosity of the proximal femur improves identification of women with nonvertebral fragility fractures. Osteoporos Int. 2015;26(8): 2137–46.
18. Arentsen L, Yagi M, Takahashi Y, et al. Validation of marrow fat assessment using noninvasive imaging with histologic examination of human bone samples. Bone. 2015;72:118–22.
19. Turner AS. The sheep as a model for osteoporosis in humans. Vet J. 2002;163(3):232–9.
20. Schindelin J, Arganda-Carreras I, Frise E, et al. Fiji: an open-source platform for biological-image analysis. Nat Methods. 2012;9(7): 676–82.
21. Bjørnerem Å, Bui QM, Ghasem-Zadeh A, Hopper JL, Zebaze R, Seeman E. Fracture risk and height: an association partly accounted for by cortical porosity of relatively thinner cortices. J Bone Miner Res. 2013;28(9):2017–26.
22. Bjørnerem Å, Bui M, Wang X, et al. Genetic and environmental variances of bone microarchitecture and bone remodeling markers: a twin study. J Bone Miner Res. 2015;30(3):519–27.
23. Laib A, Häuselmann HJ, Rüegsegger P. In vivo high resolution 3D-QCT of the human forearm. Technol Health Care. 1998;6(5-6): 329–37.
24. Bala Y, Zebaze R, Ghasem-Zadeh A, et al. Cortical porosity identifies women with osteopenia at increased risk for forearm fractures. J Bone Miner Res. 2014;29(6):1356–62.
25. Zebaze R, Ghasem-Zadeh A, Mbala A, Seeman E. A new method of segmentation of compact-appearing, transitional and trabecular compartments and quantification of cortical porosity from high resolution peripheral quantitative computed tomographic images. Bone. 2013;54(1):8–20.
26. Zebaze RM, Ghasem-Zadeh A, Bohte A, et al. Intracortical remodelling and porosity in the distal radius and post-mortem femurs of women: a cross-sectional study. Lancet. 2010;375(9727): 1729–36.
27. Looker AC, Orwoll ES, Johnston CC, et al. Prevalence of low femoral bone density in older US adults from NHANES III. J Bone Miner Res. 1997;12(11):1761–8.
28. Lawless J, Singhal K. Efficient screening of nonnormal regression models. Biometrics. 1978;34(2):318–27.
29. Peña JA, Thomsen F, Damm T, et al. Bone-marrow densitometry: assessment of marrow space of human vertebrae by single energy high resolution-quantitative computed tomography. Med Phys. 2016;43(7):4174.
30. Siris ES, Chen Y-T, Abbott TA, et al. Bone mineral density thresholds for pharmacological intervention to prevent fractures. Arch Intern Med. 2004;164(10):1108–12.
31. Wehrli F, Hopkins J, Hwang S, Song H, Snyder P, Haddad J. Cross-sectional study of osteopenia by quantitative magnetic resonance and bone densitometry. Radiology. 2000;217:527–38.
32. Yeung DKW, Griffith JF, Antonio GE, Lee FKH, Woo J, Leung PC. Osteoporosis is associated with increased marrow fat content and decreased marrow fat unsaturation: A proton MR spectroscopy study. J Magn Reson Imaging. 2005;22(2):279–85.
33. Griffith JF, Yeung DK, Antonio GE, et al. Vertebral marrow fat content and diffusion and perfusion indexes in women with varying bone density: MR evaluation. Radiology. 2006;241(3):831–8.
34. Li X, Kuo D, Schafer AL, et al. Quantification of vertebral bone marrow fat content using 3 Tesla MR spectroscopy: reproducibility, vertebral variation, and applications in osteoporosis. J Magn Reson Imaging. 2011;33(4):974–9.
35. Biver E, Durosier-Izart C, Chevalley T, van Rietbergen B, Rizzoli R, Ferrari S. Evaluation of radius microstructure and areal bone mineral density improves fracture prediction in postmenopausal women. J Bone Miner Res. 2018;33(2):328–37.
36. Seeman E. Growth and age-related abnormalities in cortical structure and fracture risk. Endocrinol Metab (Seoul). 2015;30(4):419–28.
37. Andreasen CM, Delaisse JM, Cj van der Eerden B, van Leeuwen JP, Ding M, Andersen TL. Understanding age-induced cortical porosity in women: the accumulation and coalescence of eroded cavities upon existing intracortical canals is the main contributor. J Bone Miner Res. 2018;33(4):606–20.
38. Syed FA, Oursler MJ, Hefferanm T, Peterson JM, Riggs BL, Khosla S. Effects of estrogen therapy on bone marrow adipocytes in post-menopausal osteoporotic women. Osteoporos Int. 2008;19(9):1323–30.
39. Rantalainen T, Nikander R, Heinonen A, Cervinka T, Sievänen H, Daly RM. Differential effects of exercise on tibial shaft marrow density in young female athletes. J Clin Endocrinol Metab. 2013;98(5):2037–44.
40. Belavy DL, Quittner MJ, Ridgers ND, Shiekh A, Rantalainen T, Trudel G. Specific modulation of vertebral marrow adiposity tissue by physical activity. J Bone Miner Res. 2018;33(4):651–7.
41. Bolotin H, Sievänen H. Inaccuracies inherent in dual-energy X-ray absorptiometry in vivo bone mineral density can seriously mislead diagnostic/prognostic interpretations of patient-specific bone fragility. J Bone Miner Res. 2001;16(5):799–805.
42. Bolotin H, Sievänen H, Grashuis J. Patient-specific DXA bone mineral density inaccuracies: quantitative effects of nonuniform extraosseous fat distributions. J Bone Miner Res. 2003;18(6):1020–7.